RSC Advances

ROYAL SOCIETY OF CHEMISTRY

www.rsc.org/advances

Polyacrylamide-derived carbon materials: Outstanding enhancement of supercapacitor capacitance simply by introducing redox additive of *p*-aminobenzenesulfonate into KOH electrolyte

Zhong Jie Zhang[1],*, Xuan Huang, and Xiang Ying Chen[2]

[1]*College of Chemistry & Chemical Engineering, Anhui Province Key Laboratory of Environment-friendly Polymer Materials, Anhui University, Hefei 230601, Anhui, P. R. China. * The corresponding author. E-mail: zhangzj0603@126.com.*

[2]*School of Chemistry and Chemical Engineering, Anhui Key Laboratory of Controllable Chemistry Reaction & Material Chemical Engineering, Hefei University of Technology, Hefei, Anhui 230009, P R China. E-mail: cxyhfut@gmail.com.*

Abstract

How to effectively improve the capacitances is still challenging in the field of supercapacitors. In this work, a simple but efficient redox additive of sodium *p*-aminobenzenesulfonate has been incorporated into KOH electrolyte, which can largely elevate the capacitances of carbon-based supercapacitors (produced by the template carbonization of polyacrylamide and zinc metal.). It clearly indicates that the *p*-aminobenzenesulfonate concentration in KOH electrolyte has exerted a crucial role in the determination of final capacitances as well as energy efficiency. Owing to efficient electron/proton transfer of the *p*-aminobenzenesulfonate, the **C-900-10** sample with the concentration of 10 mmol L^{-1} can deliver a much higher capacitance of 681.5 F g^{-1}, when measured at 2 A g^{-1}, which is *ca*. 2.86 times increase than that of pristine one (238.2 F g^{-1}). The present *p*-aminobenzenesulfonate is anticipated to be employed in KOH electrolyte as efficient redox additive for simply producing high performance supercapacitors.

Keywords: Polyacrylamide; Template; Nanoporous carbon materials; Redox; Sodium *p*-aminobenzenesulfonate; Supercapacitor.

1. Introduction

Currently, electrical energy storage is one of the most critical/promising areas of worldwide technological researches. Supercapacitors are so far the ideal candidates for achieving highly effective energy storages and power managements, yet they still suffer from undesirable energy densities in contrast to conventional batteries.[1] To get elevated energy densities (*e.g.*, higher than 10 Wh kg^{-1}), various kinds of research strategies, mainly including electrode materials, electrolyte species, and assemble types of supercapacitors, have been implemented.[2] As clearly indicated in the literatures, the field of electrode materials is currently undergoing an exciting development, while the others, especially the electrolyte field, have drawn less attention.[3]

Interestingly, incorporating certain amount of redox additives or mediators into the common electrolytes (such as KOH, H_2SO_4) has been recently proved to be an alternative/meaningful approach, which can largely improve the supercapacitor performances *via* redox reactions at the electrode–electrolyte interface by.[4] These redox additives or compounds are directly involved in the electron transfer redox reactions; thereby the whole performances are simply elevated by their Faradaic pseudo-capacitances. Till to now, various materials have been proposed to serve as redox additives. For example, Selvan *et al.* reported KI as redox additive in 1 M KOH electrolyte, and in the optimized 1 M KOH + 0.05 M KI electrolyte, the specific capacitance and energy density of reduced graphene oxide (rGO) is 500 F g^{-1} and 44 Wh kg^{-1}, respectively.[5] Besides, the addition of redox-active decamethylferrocene in an organic electrolyte results in an approximately 27-fold increase in the energy density of carbon nanotube-based supercapacitors.[6] A redox-active gel polymer electrolyte was prepared by introducing KI/$VOSO_4$ redox additives into a polyvinyl alcohol–H_2SO_4 gel electrolyte for application in a quasi-solid-state electrical double-layer capacitor (EDLC) based on activated carbon, exhibiting high capacitance of 1232.8 F g^{-1} and a high energy density of 25.4W h kg^{-1}.[7] Other promising redox additives include $K_3Fe(CN)_6$ in Na_2SO_4 electrolyte,[8] $CuCl_2$ in HNO_3 electrolyte,[9] $CuSO_4$ in H_2SO_4 electrolyte,[10] Na_2MoO_4 in H_2SO_4 electrolyte[11] *etc*. As a whole, further exploring novel redox additive for highly improving capacitance is still imperative for materials scientists.

Herein, we present a novel redox additive of sodium *p*-aminobenzenesulfonate that can release 1-electron and 1-proton due to the existence of amine group in the redox reaction process, which is anticipated to efficiently enhance the capacitance of

carbon-based supercapacitors. The impact of *p*-aminobenzenesulfonate concentration in KOH electrolyte on the capacitance was deeply investigated by means of cyclic voltammetry, galvanostatic charge-discharge, Nyquist plot, and cycling stability measurements.

2. Experimental

Synthesis protocol: In this work, polyacrylamide has been converted into nanoporous carbon materials containing nitrogen species in the presence of zinc metal by the template carbonization method, producing the **C-800/900/1000** samples. It is also revealed that the **C-900** sample delivers the largest capacitance among them. Furthermore, in order to continue to elevate the capacitance of the **C-900** sample, sodium *p*-aminobenzenesulfonate substance serving as redox additive that can deliver the 1-electron and 1-proton transfer reaction was added into KOH electrolyte. The sodium *p*-aminobenzenesulfonate concentrations in 6 mol L^{-1} KOH electrolyte were designated as 5, 10, and 15 mmol L^{-1}, which are named as **C-900-5**, **C-900-10**, **C-900-15**, respectively.

2.1 Typical template carbonization synthesis procedure for carbon samples.

Polyacrylamide and zinc metal with the mass ratio of 2:1 were ground in a agate mortar, and then placed in a porcelain boat, flushing with Ar flow for 30 min, and further heated in a horizontal tube furnace up to 800, 900, or 1000 ºC at a rate of 5 ºC min^{-1} and maintained at this temperature for 2 h under Ar flow. The resultant product was immersed with 1 mol L^{-1} HCl solution to remove soluble/insoluble substances, subsequently washed with adequate deionized water. Finally, the sample was dried under vacuum at 120 °C for 12 h to achieve the **C-800/900/1000** samples.

2.2 Characterization

X-ray diffraction (XRD) patterns were obtained on a Rigaku D/MAX2500V with Cu Kα radiation. Raman spectra were recorded at ambient temperature on a Spex 1403 Raman spectrometer with an argon-ion laser at an excitation wavelength of 514.5 nm.

2.3 Electrochemical measurements

A mixture of 80 wt% the carbon sample (~ 4 mg), 15 wt% acetylene black and 5 wt% polytetrafluoroethylene (PTFE) binder was fabricated using ethanol as a solvent.

Slurry of the above mixture was subsequently pressed onto nickel foam under a pressure of 20 MPa, serving as the current collector. The prepared electrode was placed in a vacuum drying oven at 120 ºC for 24 h. A three electrode experimental setup taking a 6 mol L^{-1} KOH aqueous solution as electrolyte was used in cyclic voltammetry and galvanostatic charge-discharge measurements on an electrochemical working station (CHI660D, ChenHua Instruments Co. Ltd., Shanghai). Here, the prepared electrode, platinum foil (6 cm^2) and saturated calomel electrode (SCE) were used as the working, counter and reference electrodes, respectively.

Specific capacitances derived from galvanostatic tests can be calculated from the equation:

$$c = \frac{I\mathrm{d}t}{m\mathrm{d}U}$$

where C (F g^{-1}) is the specific capacitance; I (A) is the discharge current; t (s) is the discharge time; U (V) is the voltage window; and m (g) is the mass of active materials loaded in working electrode.

Specific capacitances derived from cyclic voltammetry tests can be calculated from the equation:

$$C = \frac{1}{mv(U_{\mathrm{b}} - U_{\mathrm{a}})} \int_{U_{\mathrm{a}}}^{U_{\mathrm{b}}} I\mathrm{d}U$$

where C (F g^{-1}) is the specific capacitance; m (g) is the mass of active materials loaded in working electrode; v (V s^{-1}) is the scan rate; I (A) is the discharge current; U_{b} and U_{a} (V) are high and low voltage limit of the CV tests.

3. Results and discussion

In present work, we chose commercially available polyacrylamide as carbon source, and zinc metal (being in a powder state) as hard template. These mixtures were further heated under the temperatures of 800, 900, or 1000 ºC, resulting in the formation of **C-800/900/1000** samples. The whole synthesis process is named after template carbonization method, which is a powerful tool for producing carbon materials with precisely controlled structures at the nanometer level.[10] Our research group has recently produced a series of nanoporous carbon materials *via* the template carbonization method, in particular assisted with the help of low melting metal powders,

such as Zn, Mg, and Al metals in powder state.[11,12] The reason we selected Zn, Mg, and Al metals as hard templates mostly lie in the following aspects: first, their melting points (419, 670 and 659 ºC towards Zn, Mg, and Al bulk materials, respectively) are relatively low, making them possibly melting synchronously (even before) with the carbonization of carbon precursors, which guarantee their effective template effect on the formation of nanoscale pores within carbon matrix; secondly, their derivative oxide states (ZnO, MgO, Al_2O_3) after carbonization treatment, especially the former two ones, can be readily removed by the non-corrosive/environmentally friendly acid such as HCl (instead of corrosive acid of HF commonly for removing silica template). Herein, the schematic drawing for the production of nanoporous carbon materials derived from polyacrylamide and zinc metal is briefly depicted in Fig. 1a. Moreover, the polyacrylamide is a polymer ($-CH_2CHCONH_2-$) formed from acrylamide subunits, which can serve as excellent carbon precursor for producing nanoporous carbon materials.

Concerning the as-obtained **C-800/900/1000** samples, the structure characteristics such as composition, crystallinity, and purity were briefly revealed by XRD technique. Fig. 1b indicates the representative XRD patterns of the **C-800/900/1000** samples, all of which exhibit one broad and low-intensity diffraction peak located at 24.9º. Apparently, these peaks imply the amorphous features, which can be approximately indexed as (002) plane of crystalline graphite. Of course, the amorphous natures have also been confirmed by their obvious shifts of 2 theta value (24.9º), compared to that of the standard graphite (commonly as 26.6º). What's more, one thing that needs to be noted is that the peak configurations of the **C-800/900/1000** samples are actually different in a minor manner, whose peaks largely decrease in intensities with the incremental growth of carbonization temperatures from 800 to 1000 º C. That is to say, higher carbonization temperature favors for the occurrence of carbon materials with larger graphitization.[13]
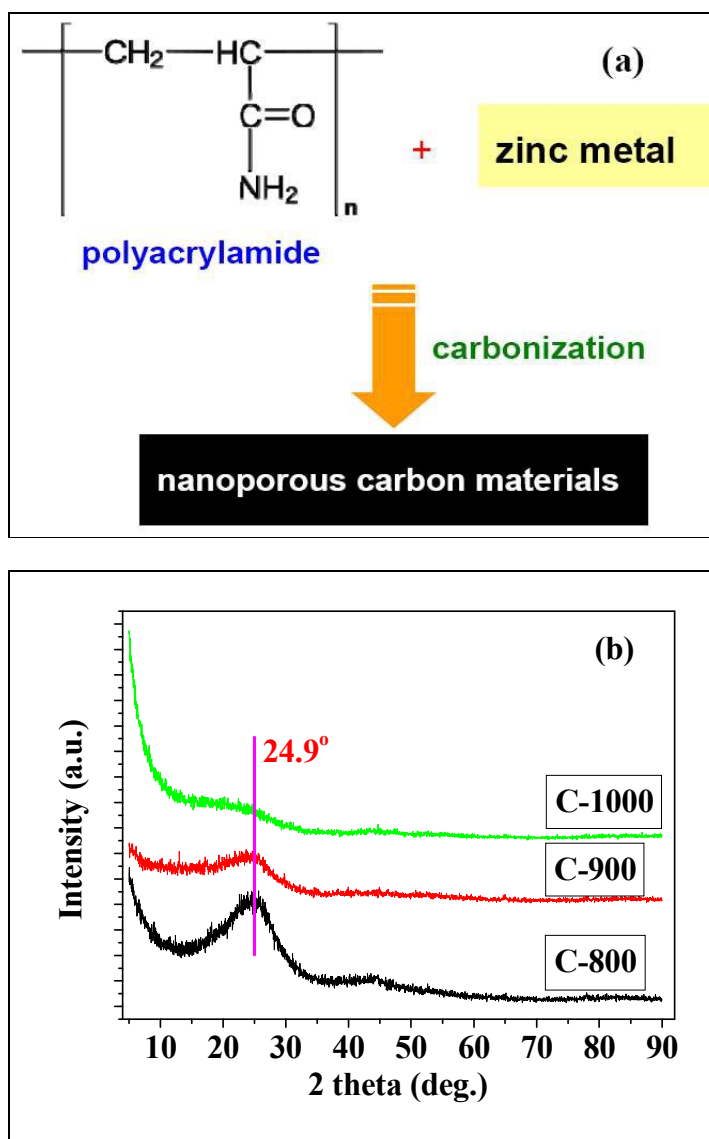
Fig. 1. (a) Schematic drawing for the production of nanoporous carbon materials; and XRD patterns of the (b) **C-800**, (c) **C-900**, and (d) **C-1000** samples.

On the other hand, Raman spectroscopy is capable of discerning even slight changes in carbon structures, making it a very valuable tool in the characterization of carbon nanomaterials such as amorphous carbon, carbon nanotubes, and graphene *etc*. Fig. 2 indicates the typical Raman spectra of the **C-800/900/1000** samples with a large wavenumber range of $500 \sim 3500$ cm^{-1}. Clearly, there exists two Raman peaks (not completely discrete each other) at $1342.2 \sim 1343.4$ cm^{-1}, and $1598.5 \sim 1603.3$ cm^{-1}, respectively. The former peaks, usually named as D band (in more details, it can be

deconvoluted into four independent peaks of D1, D2, D3, and D4), are attributed to disorder graphitic carbon and/or amorphous carbon; besides, the latter peaks correspond to ideal graphitic lattices.[14] Notably, all of the present G bands have shifted ~ 20 cm^{-1} toward higher wavenumber, compared to that of the ideal graphite (commonly at 1580 cm^{-1}), which are probably due to the nanoscale crystalline carbon sizes of the e **C-800/900/1000** samples.[15]

As is well known, the intensity ratio of D band to G band (I_D/I_G) is a convincing protocol to determine the graphitization degree (*e.g.* crystallinity) of carbon materials. Herein, the I_D/I_G values are of 1.06, 0.93, and 1.04 towards the cases of the **C-800/900/1000** samples, respectively, also indicating their amorphous features (primarily complying with the XRD results). Gogotsi *et al*. once reported the nanoporous carbide-derived carbon synthesis from the chlorination of carbides (such as Ti$_3$SiC$_2$, SiC *etc*), in which pronounced graphitization is observed only at 1200 °C, resulting in a sharper G-band in the Raman spectrum and decreased I_D/I_G ratio.[16] In other words, the I_D/I_G ratio still increase from 0.95 to 1.4 when the chlorination/carbonization temperatures elevating from 200 to 1100 °C, but it suddenly decrease to be 0.4 when the temperature approaches to 1200 °C. Thereby, the carbonization temperature is a crucial factor that determines the graphitization degree of carbon materials.
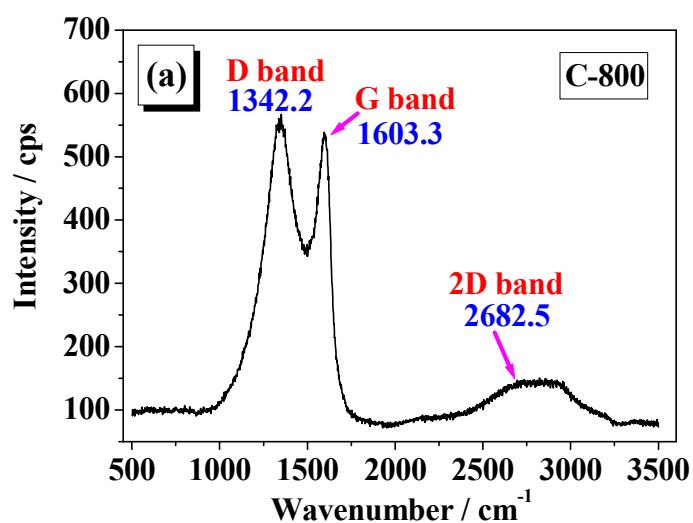
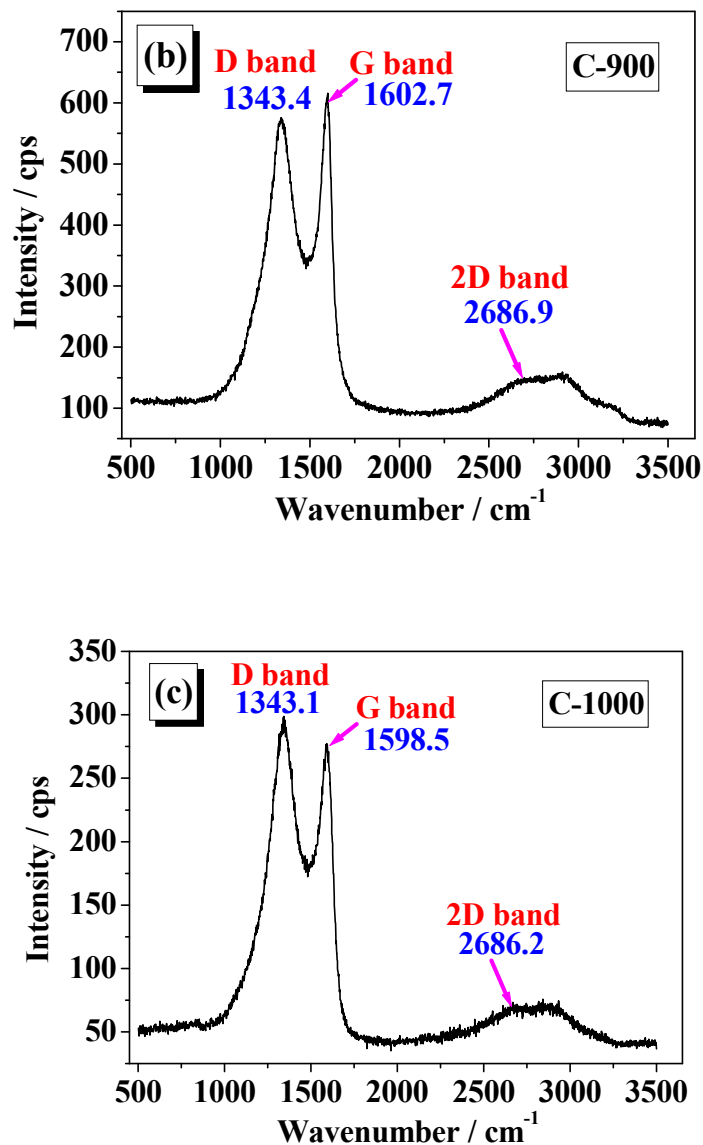**Fig. 2**. Raman spectra of the (b) **C-800**, (c) **C-900**, and (d) **C-1000** samples.

The electrochemical performances of the **C-800/900/1000** samples were first measured in a three-electrode system, using 6 mol L^{-1} KOH as pristine electrolyte. Fig. 3a indicates the contrast CV curves of the **C-800/900/1000** samples when designated at 100 mV s^{-1} in a voltage window of -1.0 ~ 0 V. Basically, the three cyclic voltammetry (*abbr*. CV) curves display approximate rectangular configurations without obvious redox peaks, clearly revealing their feature of electrical double layer capacitances

(EDLCs). That is to say, the contribution of pseudo-capacitances among these overall capacitances is quite minor, which is a kind of commonsense towards carbon-based supercapacitors. On the other hand, the order of these integral areas is as follows: **C-900 > C-1000 > C-800**. Consequently, the specific capacitance order also has the similar trend: **C-900 > C-1000 > C-800** since they are usually proportional to their integral areas. Fig. 3b shows the specific capacitances calculated from CV curves of the **C-800/900/1000** samples, and all of which exhibit high capacitances. For example, their capacitances are of 441.4, 361.2, and 299.8 F g^{-1} when estimated at the scan rate of 5 mV s^{-1}.

Besides, the galvanostatic charge-discharge (*abbr*. GCD) measurements were also carried out towards the **C-800/900/1000** samples. The three GCD curves measured at 10 A g^{-1} are displayed in Fig. 3c, also with a voltage window of -1.0 ~ 0 V. And all of them indicate nearly triangular configurations, further implying the predominant EDLCs features. In addition, we can see from Fig. 3d that the **C-900** sample delivers the largest capacitances, while those of the **C-800** sample are of the worst. For instance, when designated at 1 A g^{-1}, the **C-900** sample has the higher capacitance of 305.3 F g^{-1} but the other **C-800/1000** samples exhibit the ones of 217.7, and 225.8 F g^{-1}, respectively. This kind of correlative feature (not linear relationship) between carbonization temperature and capacitances has been previously illustrated in the cases of diphenylcarbazide-Mg(OH)$_2$,[17] MgO-templated carbon nanocages,[18] and the system of Mg citrate coexistent with Mg powder.[19]

On the other hand, coulombic efficiency (also called Faradaic efficiency) usually describes the efficiency with which charge (electrons) are transferred in a system, thus facilitating an electrochemical reaction. Regarding an ideal EDLC, coulombic efficiency (η) was calculated using the following equation: $\eta_t = \Delta t_d / \Delta t_c$, where Δt_c and Δt_d are the charging and discharging time, respectively. However, in case of non-linear GCD characteristics, coulombic efficiency (η_t) and energy efficiency (η_E) can differ significantly. Therefore, energy efficiency should be evaluated from: $\eta_E = E_{int/d} / E_{int/c}$, where the discharge energy ($E_{int/d}$) should be calculated by integrating, *i.e.* finding the area under the GD curve and the charge energy $E_{int/C}$ from GC.[20] Hence, in present work, based on the GCD curves (with slightly distorted triangular shapes, i.e., non-linear GCD characteristics) shown in Figure 3c, we can discern the energy efficiencies at 10 A g^{-1} of the **C-800/900/1000** samples should be

calculated using the latter equation: $\eta_E = E_{int/d} / E_{int/c}$, and the results are *ca*. 72.6%, 85.9%, and 81.3%, respectively. That is to say, the **C-900** sample delivers the highest energy efficiency.

Long-term cycling stability is another tremendous factor for the determination of the practical application of supercapacitors. The cycling stabilities of the **C-800/900/1000** samples were evaluated by repeating the GCD tests at a current density of 10 A g^{-1} for 5000 cycles, and the results are shown in Figure 3e. After 5000 cycles, the capacitance retention of the **C-800/900/1000** samples has retained 89.5%, 91.2%, and 94.9%, respectively, compared to the pristine capacitances. Clearly, regarding the cycling stability, the higher crystallinity/graphitization (testified by Raman results in present work) usually contributes to the larger conductivity and faster electron transport, which can lead to better cycling stability of carbon material.[21] Similar cycling stability results also occur in the case of highly graphitic clew-like nanocarbons synthesized through a simple hydrothermal method followed by impregnation and catalytic graphitization at 900 °C, in which sucrose and nickel acetate were employed as the carbon source and nickel catalyst precursor, respectively.[22]

Nyquist plots representatively exhibit the frequency response of the carbon-based electrode/electrolyte system and are a plot of the imaginary component (Z″) of the impedance against the real component (Z′). Fig. 3f shows the Nyquist plots of the 1st and 5000th cycles towards the **C-800/900/1000** samples, and all of the curves appear as straight lines at low frequency and an arc in the high frequency region. As is well known, a higher equivalent series resistance (ESR) shifts the capacitive charge process toward the higher resistance and limits the response time of the supercapacitor, especially for fast charge/discharge rates.[23] Clearly, the **C-800** sample delivers the largest ESR data, while the others of **C-900/1000** samples exhibit smaller ESR data (and both of them are almost quantitatively the same), revealing that the resistance order between them is nearly as follows: **C-800 > C-900 ≈ C-1000**. The ESR tendency among them is also evinced by the inconspicuous arc in the high frequency region, which is usually proportional to the electronic resistance.[24]
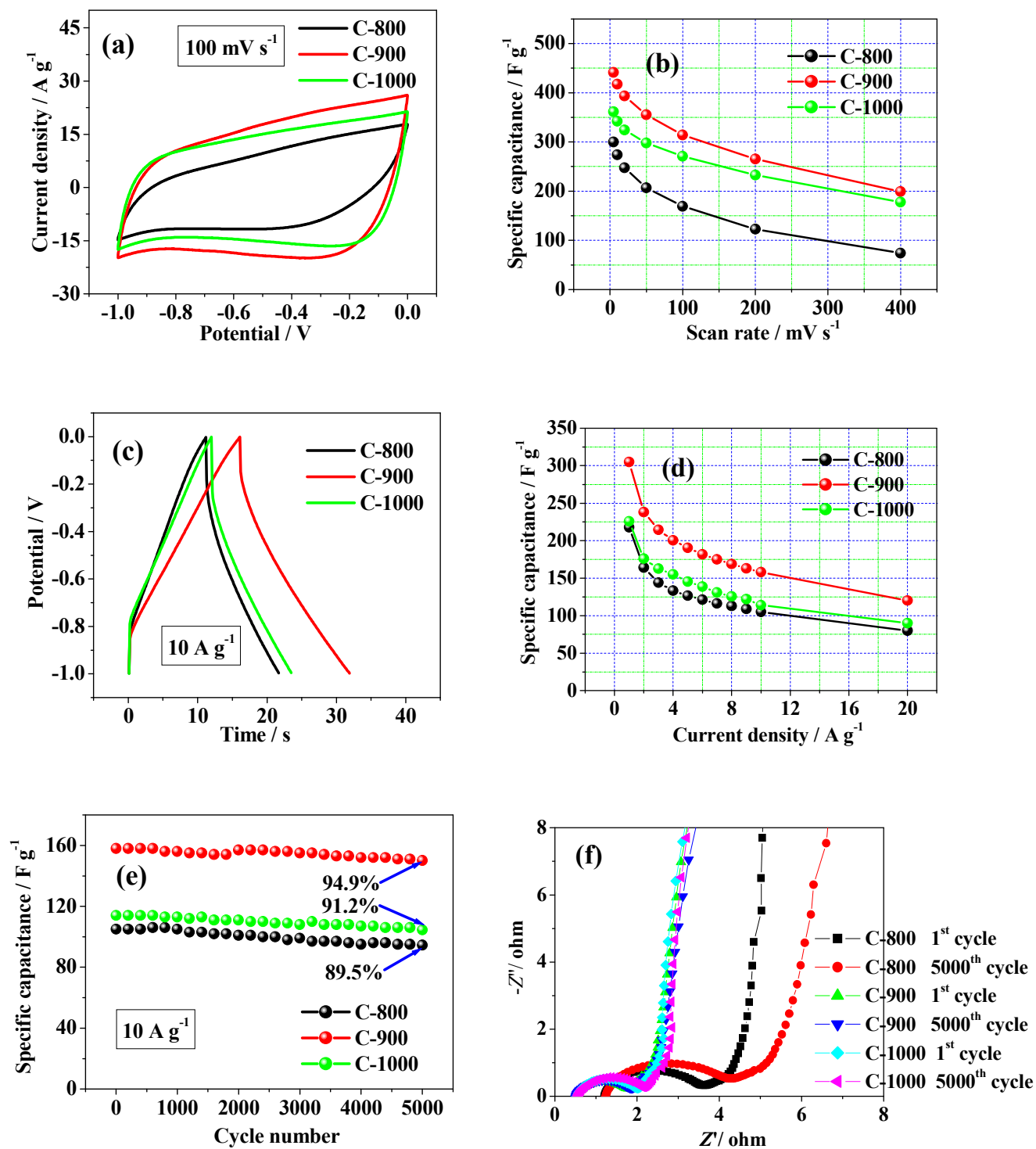
Fig. 3. The **C-800/900/1000** samples: (a) CV curves at 100 mV s^{-1}; (b) specific capacitances calculated from CV curves; (c) GCD curves at 10 A g^{-1}; (d) specific capacitances calculated from GCD curves; (e) cycling stabilities measured at 10 A g^{-1}; (f) Nyquist plots of the 1st and 5000th cycles.

Currently, how to acquire high energy density supercapacitors is a fairly interesting but challenging issue for material scientists.[2] Based on the equation of energy density: $E = \frac{1}{2}CV^2$, it is apparent that an alternative and effective approach to improving the energy density (E) is elevating the capacitance (C). As is widely documented, the enhancement of capacitance by pseudo-capacitive charge storage can be also achieved by the application of redox-active electrolytes, instead of using the electrode material as a source of redox reactions.[3] In the case of redox additive, the electrolyte is the main source of capacitance because of various oxidation states of the electrolytic species. Considering the fact that the Faradaic reactions primarily occur at the interface of electrode and electrolyte, it is interesting to select a rational but efficient redox additive that can be readily and stably incorporated into KOH electrolyte. In this work, we demonstrate a simple but effective redox additive of *p*-aminobenzenesulfonate to highly improve the capacitances, since the amine group correlative phenyls is indispensable for producing pseudo-capacitive performance.[25,26] The amine group has been proved to be crucial factor that determines the degree of redox reactions, and the excellent sample concerning amine-based redox additive is *p*-phenylenediamine. Cyclic voltammetry of *p*-phenylenediamine in the pH 7.0 phosphate buffer solution (PBS) shows a reversible anodic peak (A_0) and cathodic peak (C_0) at $E_{1/2}$ = 0.172 V, corresponding to the redox couple of p-phenylenediamine/*p*-phenylenediimine), consistent with the 2-electrons and 2-proton transfer reaction.[27] Herein, the representative redox reaction in mixed *p*-aminobenzenesulfonate-KOH electrolyte, as well as the proton/electron transfer process between the oxidation and reduction states is simply indicated in Fig. 4.
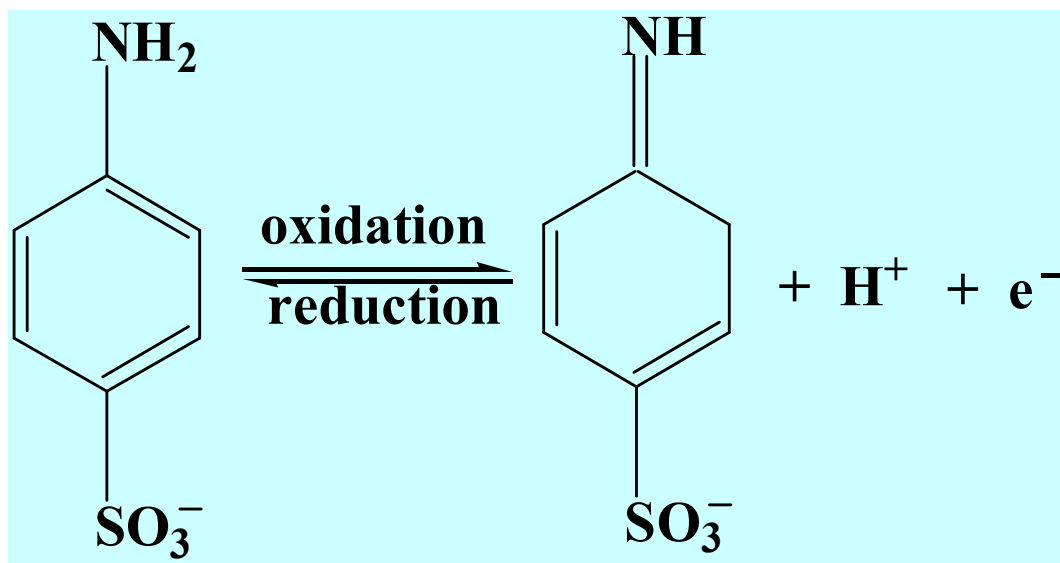
Fig. 4. Redox reaction in mixed *p*-aminobenzenesulfonate-KOH electrolyte, accompanied with one proton and one electron transfer between the oxidation and reduction states.

When designated the sodium *p*-aminobenzenesulfonate concentrations in 6 mol L^{-1} KOH electrolyte as 5, 10, and 15 mmol L^{-1}, we can obtain the **C-900-5**, **C-900-10**, **C-900-15** samples, respectively. Fig. 5a, c and e display the CV curves of the **C-900-5/10/12** samples at the scan rates of 20 ~ 400 mV s^{-1}, while keeping the voltage window of -1.0 ~ 0 V. It is clearly seen that, at low scan rates such as 20 ~ 100 mV s^{-1}, the CV curves exhibit obvious redox peaks mostly incurred by the oxidation and reduction states of *p*-aminobenzenesulfonate in 6 mol L^{-1} KOH electrolyte, while these humps gradually become ambiguous in shapes at higher scan rates of 200 ~ 400 mV s^{-1}. Note that this kind of CV redox peaks shifting (in details, the oxidation peaks shifting positively, and the reduction peaks shifting negatively) when increasing the scan rates has been commonly reported, such as the case of redox-mediated 0.6 g Na_2MoO_4 into 40 mL 1M H_2SO_4 as a mixture electrolyte.[28] It indicates the occurrences of better electrochemical and redox process between the electrode-electrolyte interface.[29] On the other hand, the GCD curves of the **C-900-5/10/12** samples at current density of 2 ~ 20 A g^{-1} are shown in Fig. 5b, d, and f. Apparently, there exists an evident platform on the charging and discharge curve, respectively, especially at low current density of 2 ~ 10 A g^{-1}.
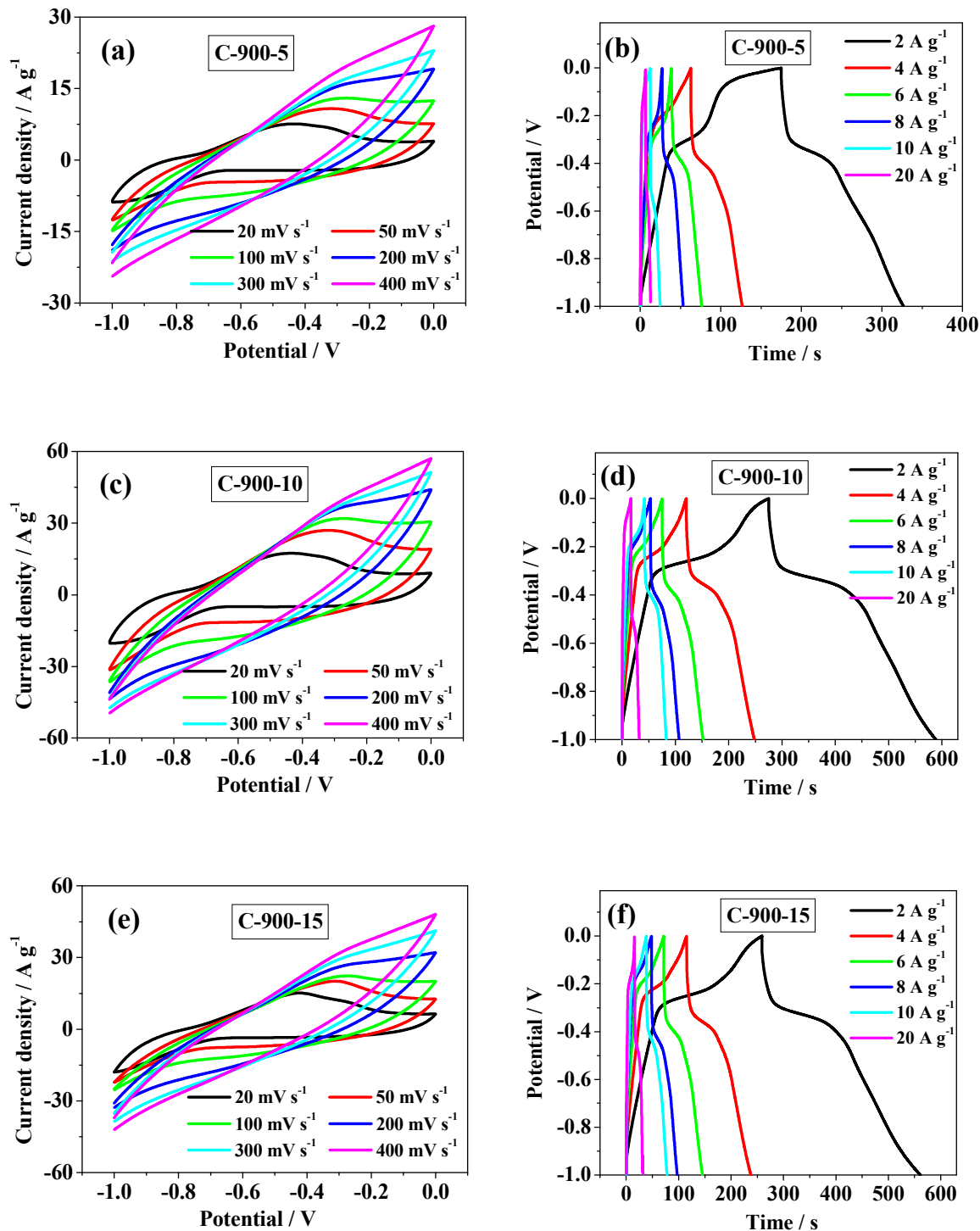
Fig. 5. The **C-900-5/10/12** samples: (a, c, e) CV curves; (b, d, f) GCD curves.

Next, the CV curves of the **C-900**, and **C-900-5/10/15** samples when measured at

20 mV s^{-1} are comparatively displayed in Fig. 6a, also fixing a voltage window of -1.0 ~ 0 V. From the viewpoint of CV configurations, it is clearly discerned that the **C-900** sample with nearly rectangular profile exhibits typical EDLC feature, while the others of **C-900-5/10/15** samples indicate obvious redox peaks, revealing their pseudo-capacitive natures resulted from the introduction of *p*-aminobenzenesulfonate. In addition, as is clearly seen in Fig. 6a, introducing *p*-aminobenzenesulfonate into KOH electrolyte has largely increased the CV integral areas, especially the cases of the **C-900-10/15** samples. Similar change results after introducing *p*-aminobenzenesulfonate into KOH electrolyte also happen towards GCD curves, as shown in Fig. 6b. Clearly, the contribution of EDLC predominantly occurs for the case of the **C-900** sample with almost linear charging-discharging lines. However, the **C-900-10/15** samples consist of large amounts of pseudo-capacitances due to their non-linear charging-discharging lines (*i.e.*, platforms). Longer charge-discharge times for the **C-900-10/15** samples than the pristine **C-900** sample could be ascribed to the additional contribution of a quick reversible redox process by *p*-aminobenzenesulfonate, as being illustrated aforementioned. So, in cases of the **C-900-10/15** samples, their overall supercapacitor capacitances are composed of EDLCs from the electrolyte ions within the pore surfaces of carbon electrodes and pseudo-capacitances achieved by *p*-aminobenzenesulfonate on the electrolyte-electrode interfaces.

Besides, based on the GCD curves with non-linear characteristics shown in Fig. 6b, the energy efficiency clearly are calculated from the equation: $\eta_E = E_{int/d} / E_{int/c}$. As a result, the energy efficiencies of the **C-900-5/10/15** samples with the different incorporation of *p*-aminobenzenesulfonate are of 66.1%, 77.4%, and 76.6% when measured at a current density of 2 A g^{-1}, respectively, which much lower than that of the pristine **C-900** sample without adding redox additive (*ca*. 99.1%). It is obvious to us that introducing *p*-aminobenzenesulfonate into KOH electrolyte can largely decrease the energy efficiency of carbon materials.

Fig. 6c depicts the specific capacitances calculated from GCD curves regarding the **C-900**, and **C-900-5/10/15** samples. Basically, introducing 5 mmol L^{-1} *p*-aminobenzenesulfonate into 6 mol L^{-1} KOH electrolyte (the case of **C-900-5** sample) has slightly enhanced the capacitances, while further increasing the amount of *p*-aminobenzenesulfonate such as 10 or 15 mmol L^{-1} into 6 mol L^{-1} KOH electrolyte (the cases of **C-900-10/15** sample) can largely increase the capacitances. For instance,

when fixed at a current density of 2 A g^{-1}, the capacitances of the **C-900**, and **C-900-5/10/15** samples are of 238.2, 344.4, 681.5, and 627.3 F g^{-1}, respectively. In other words, the increase times concerning the **C-900-5/10/15** samples have reached up to 1.45, 2.86, and 2.63, respectively, compared to the pristine one of **C-900** sample. Clearly, the **C-900-10** sample exhibits the largest capacitance among them. What's more, as clearly learned from Fig. 6c, the capacitance increase is non-linear to the dosage of *p*-aminobenzenesulfonate, which was also reported in other cases such as redox-mediated gel polymer (PVA-KOH-*p*-phenylenediamine) as electrolyte,[26] commonly correlative with the adjustment of ionic conductivity (*i.e.*, charge transfer resistance) in mixed electrolyte.[29] Besides, the comparison of the incremental capacitances by adding redox additives is typically listed in Table 1, also suggesting the superior electrochemical performance towards the present work, especially the case of **C-900-10** sample.

Furthermore, cycling stabilities of the **C-900**, and **C-900-5/10/15** samples when measured at 20 A g^{-1} are displayed in Fig. 6d. The **C-900** sample indicates the excellent cycling stability of 94.3% in contrast to the initial one, even after long-term 5000 cycles. As for the **C-900-5/10/15** samples, their cycling stabilities after charging-discharging for 5000 cycles are of 63.5%, 69.1%, and 66.2%, respectively. Clearly, the **C-900-10** sample delivers the largest capacitance retention among them. As a whole, the introduction of *p*-aminobenzenesulfonate into KOH electrolyte leads to the deterioration of cycling stability, which might be due to the reduction of electrical conductivity in mixed electrolyte, as well as the resultant insufficient redox reaction between the oxidation and reduction states of *p*-aminobenzenesulfonate after long charge–discharge cycle.[24] Similar research result also happens in the case of the supercapacitor based on a novel redox-mediated gel polymer electrolyte (PVA-H$_2$SO$_4$-P-benzenediol) and activated carbon electrodes.[29] In addition, the cycling stabilities of the **C-900**, and **C-900-5/10/15** samples are also evinced by the GCD curves and Nyquist plots of the 1st and 5000th cycles, as shown in Fig. 6e, and 6f, respectively. Notably, the redox additive must exhibits a rapid electron exchange kinetic at the electrode/electrolyte interface so that the coulombic efficiency would be quite high, indicating firstly, that the entire electrolyte is stable during the charge–discharge cycles and secondly, that all the molecules oxidized during the charge process are reduced over the discharge.
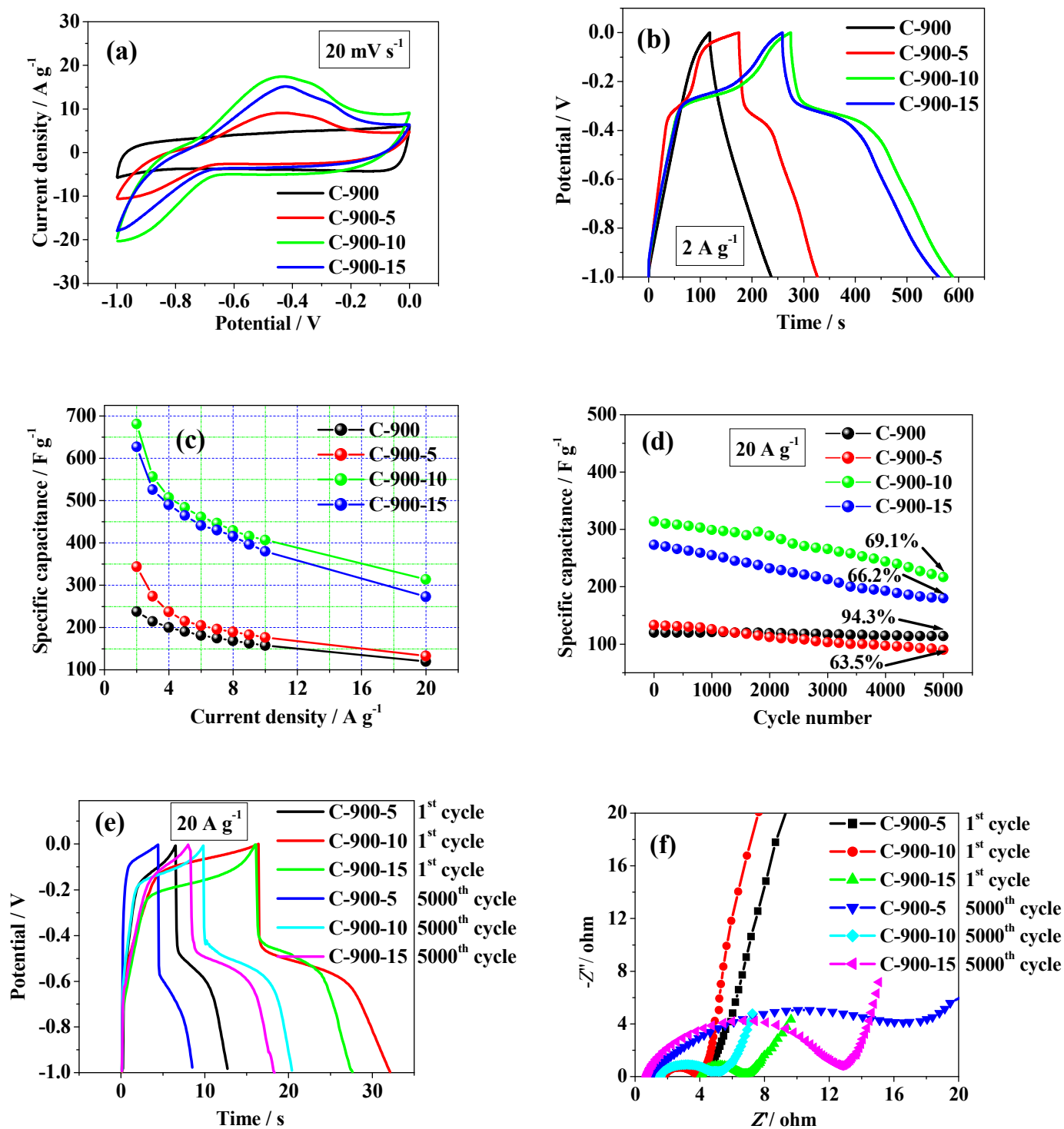
Fig. 6. The **C-900**, and **C-900-5/10/15** samples: (a) CV curves at 20 mV s^{-1}; (b) GCD curves at 2 A g^{-1}; (c) specific capacitances calculated from GCD curves; (d) cycling stabilities measured at 20 A g^{-1}; (e) GCD curves of the 1st and 5000th cycles; (f) Nyquist plots of the 1st and 5000th cycles.

Table 1. Comparison of the incremental capacitances by adding redox additives.

Redox additive	C_s (F g^{-1})		Current density	Ref.
	Pristine	After adding redox additive		
p-phenylenediamine	144.0	605.2	1 A g^{-1}	25
KI	472	912	2 mA cmg^{-2}	29
m-phenylenediamine	36.4	78.01	0.5A g^{-1}	31
hydroquinone	42.2	72.3	1 A g^{-1}	32
hydroquinone	320.0	901.0	2.65 mA cmg^{-2}	33
p-aminobenzenesulfonate	238.2	627.3	2 A g^{-1}	**present work**

5. Conclusions

In summary, we demonstrate a simple but effective redox additive of sodium *p*-aminobenzenesulfonate to largely improve the capacitance of carbon-based supercapacitors, which was produced by the template carbonization of polyacrylamide and zinc metal. It is revealed that the *p*-aminobenzenesulfonate concentration in KOH electrolyte has a crucial role in the determination of final capacitances of supercapacitors, in terms of a series of electrochemical measurements techniques, mainly including CV/GCD curves, Nyquist plot, and cycling stability. Besides, the redox reaction of *p*-aminobenzenesulfonate in KOH electrolyte has also been illustrated, accompanied with proton/electron transfer between the oxidation and reduction states.

From a panoramic view, there exist many scientific merits in the present work, which will be briefly illustrated as follows: (1) commercially available polyacrylamide has been converted into amorphous but nanoporous carbon materials through a straightforward template carbonization method, using zinc metal as hard template; (2) Introducing certain amount of sodium *p*-aminobenzenesulfonate into KOH electrolyte can largely elevate the capacitances as well as the energy efficiency, primarily due to the fact that sodium *p*-aminobenzenesulfonate serving as redox additive can release 1-electron and 1-proton due to the existence of amine group in the redox reaction process. For example, the **C-900-10** sample delivers a much higher capacitance of 681.5 F g^{-1}, when measured at 2 A g^{-1}, which is ca. 2.86 times than that of pristine one (238.2 F g^{-1}); (3) the present sodium *p*-aminobenzenesulfonate acting as redox additive is

inexpensive, environmentally friendly, and, in particular, the operation for improving the capacitance by introducing redox additive into KOH electrolyte can be easily carried out at ambient conditions, and all of these advantages make it possible for its practical application in high electrochemical performance (especially with large energy density) supercapacitor fields.

6. Acknowledgments

7. References

1 L. L. Zhang and X. S. Zhao, *Chem. Soc. Rev.*, 2009, **38**, 2520–2531.

2 J. Yan, Q. Wang, T. Wei and Z. Fan, *Adv. Energy Mater.*, 2014, **4**, DOI: 10.1002/aenm.201300816.

3 F. Béguin, V. Presser, A. Balducci and E. Frackowiak, *Adv. Mater.*, 2014, **26**, 2219–2251.

4 S. T. Senthilkumar, R. K. Selvan and J. S. Melo, *J. Mater. Chem. A*, 2013, **1**, 12386–12394.

5 K. V. Sankar and R. K. Selvan, *Carbon*, 2015, **90**, 260–273.

6 J. Park, B. Kim, Y. Yoo, H. Chung and W. Kim, *ACS Appl. Mater. Interfaces*, 2014, **6**, 19499−19503.

7 L. Q. Fan, J. Zhong, J. H. Wu, J. M. Lin and Y. F. Huang, *J. Mater. Chem. A*, 2014, **2**, 9011–9014.

8 K. Chen, F. Liu, D. Xue and S. Komarneni, *Nanoscale*, 2015, **7**, 432–439.

9 L. Q. Mai, A. M. Khan, X. Tian, K. M. Hercule, Y. L. Zhao, X. Lin and X. Xu, *Nat. Commun.*, 2013, **4**, 2923: 1-7.

10 H. Nishihara and T. Kyotani, *Adv. Mater.*, 2012, **24**, 4473−4498.

11 X. Y. Chen, L. X. Cheng, X. Deng, L. Zhang and Z. J. Zhang, *Ind. Eng. Chem. Res.*, 2014, **53**, 6990−6997.

12 Z. J. Zhang, X. Y. Chen, D. H. Xie, P. Cui and J. W. Liu, *J. Mater. Chem. A*, 2014, **2**, 9675−9683.

13 J. Zhou, Z. Zhang, W. Xing, J. Yu, G. Han, W. Si and S. Zhuo, *Electrochim. Acta*, 2015, **153**, 68−75.

14 A. Sadezky, H. Muckenhuber, H. Grothe, R. Niessner and U. Poschil, *Carbon*, 2005, **43**, 1731−1742.

15 H. Zhang, X. Zhang, X. Sun and Y. Ma, *Sci. Rep.*, 2014, **3**, 3534, DOI: 10.1038/srep03534.

16 Y. Gogotsi, A. Nikitin, H. Ye, W. Zhou, J. E. Fischer, B. Yi, H. C. Foley and M. W. Barsoum, *Nat. Mater.*, 2003, **2**, 591−594.

17 X. Y. Chen, L. Zhang, L. X. Cheng, Y. Y. He and Z. J. Zhang, *Electrochim. Acta*, 2014, **142**, 84−91.

18 K. Xie, X. Qin, X. Wang, Y. Wang, H. Tao, Q. Wu, L. Yang and Z. Hu, *Adv. Mater.*, 2012, **24**, 347−352.

19 Y. Q. Zhu, H. T. Yi, X. Y. Chen and Z. H. Xiao, *Ind. Eng. Chem. Res.*, 2015, **54**, 4956−4964.

20 A. Laheäär, P. Przygochi, O. Abbas, F. Béguin, *Electrochem. Commun.*, 2015, **60**, 21−25.

21 L. Sun, C. Tian, Y. Fu, Y. Yang, J. Yin, L. Wang and H. Fu, *Chem. Eur. J.*, 2014, **20**, 564−574.

22 T. Liu, E. Liu, R. Ding, Z. Luo, T. Hu and Z. Li, *ChemElectroChem*, 2015, **2**, 852−858.

23 P. L. Taberna, P. Simon, J. F. Fauvarque, *J. Electrochem. Soc.*, 2003, **150**, A292−A300.

24 Y. Wang, Z. Shi, Y. Huang, Y. Ma, C. Wang, M. Chen and Y. Chen, *J. Phys. Chem. C*, 2009, **113**, 13103−13107.

25 J. Wu, H. Yu, L. Fan, G. Luo, J. Lin and M. Huang, *J. Mater. Chem.*, 2012, **22**, 19025–19030.

26 G. Ma, E. Fang, K. Sun, H. Peng, J. Li and Z. Lei, *Electrochim. Acta*, 2014, **135**, 461–466.

27 N. J. Ke, S. S. Lu, S. H. Cheng, *Electrochem. Commun.*, 2006, **8**, 1514–1520.

28 K. Sun, E. Feng, H. Peng, G. Ma, Y. Wu, H. Wang and Z. Lei, *Electrochim. Acta*, 2015, **158**, 361–367.

29 S. T. Senthilkumar, R. K. Selvan, Y. S. Lee and J. S. Melo, *J. Mater. Chem. A*, 2013, **1**, 1086–1095.

30 H. Yu, J. Wu, L. Fan, Y. Lin, K. Xu, Z. Tang, C. Cheng, S. Tang, J. Lin, M. Huang, Z. Lan, *J. Power Sources*, 2012, **198**, 402–407.

31 H. Yu, L. Fan, J. Wu, Y. Lin, M. Huang, J. Lin and Z. Lan, *RSC Adv.*, 2012, **2**,

6736–6740.

32 S. Sathyamoorthi, V. Suryanarayanan and D. Velayutham, *J. Power Sources*, 2015, **274**, 1135–1139.

33 S. Roldán, C. Blanco, M. Granda, R. Menéndez and R. Santamaría, *Angew. Chem. Int. Ed.*, 2011, **50**, 1699–1701.